JEM

Article

Cilia loss sensitizes cells to transformation by activating the mevalonate pathway

Yue-Zhen Deng,[1,4] Zhen Cai,[1] Shuo Shi,[1] Hao Jiang,[1] Yu-Rong Shang,[1] Ning Ma,[1] Jing-Jing Wang,[1] Dong-Xian Guan,[1] Tian-Wei Chen,[1] Ye-Fei Rong,[5] Zhen-Yu Qian,[1] Er-Bin Zhang,[1] Dan Feng,[1] Quan-Li Zhou,[3] Yi-Nan Du,[7] Dong-Ping Liu,[1] Xing-Xu Huang,[7] Lu-Ming Liu,[6] Eugene Chin,[3] Dang-Sheng Li,[2] Xiao-Fan Wang,[8] Xue-Li Zhang,[9] and Dong Xie[1]

[1]Key Laboratory of Nutrition and Metabolism, Institute for Nutritional Sciences and [2]Shanghai Institute of Biochemistry and Cell Biology, Shanghai Institutes for Biological Sciences, Chinese Academy of Sciences, Shanghai, China
[3]Institute of Health Sciences, Shanghai Institutes for Biological Sciences, Chinese Academy of Sciences, Shanghai Jiaotong University School of Medicine, Shanghai, China
[4]Center for Molecular Medicine, Xiangya Hospital, Central South University, Changsha, China
[5]Pancreatic Cancer Group, General Surgery Department, Zhongshan Hospital and [6]Department of Oncology, Shanghai Medical College, Fudan University, Shanghai, China
[7]School of Life Science and Technology, Shanghai Tech University, Shanghai, China
[8]Department of Pharmacology and Cancer Biology, Duke University Medical Center, Durham, NC
[9]Department of General Surgery, Fengxian Hospital Affiliated to Southern Medical University, Shanghai, China

Although cilia loss and cell transformation are frequently observed in the early stage of tumorigenesis, the roles of cilia in cell transformation are unknown. In this study, disrupted ciliogenesis was observed in cancer cells and pancreatic cancer tissues, which facilitated oncogene-induced transformation of normal pancreatic cells (HPDE6C7) and NIH3T3 cells through activating the mevalonate (MVA) pathway. Disruption of ciliogenesis up-regulated MVA enzymes through β catenin–T cell factor (TCF) signaling, which synchronized with sterol regulatory element binding transcription factor 2 (SREBP2), and the regulation of MVA by β-catenin–TCF signaling was recapitulated in a mouse model of pancreatic ductal adenocarcinoma (PDAC) and human PDAC samples. Moreover, disruption of ciliogenesis by depleting *Tg737* dramatically promoted tumorigenesis in the PDAC mouse model, driven by $Kras^{G12D}$, which was inhibited by statin, an inhibitor of the MVA pathway. Collectively, this study emphasizes the crucial roles of cilia in governing the early steps of the transformation by activating the MVA pathway, suggesting that statin has therapeutic potential for pancreatic cancer treatment.

The Journal of Experimental Medicine

INTRODUCTION

Alteration in cellular metabolism is one of the hallmarks of cancer cells (Hsu and Sabatini, 2008; Hanahan and Weinberg, 2011). Many key oncogenic signaling pathways converge to regulate metabolism in order to facilitate the survival and growth of cancer cells (Israelsen and Vander Heiden, 2010; Lyssiotis and Cantley, 2012). The mevalonate (MVA) pathway is involved in the production of several fundamental metabolites, including cholesterol, isoprenoids, and ubiquinone (Gruenbacher and Thurnher, 2015). The rate-limiting enzyme 3-hydroxy-3-methylglutaryl coenzyme A reductase (HMGCR) is tightly regulated by sterol regulatory element-binding transcription factor 2 (SREBP2; Popják et al., 1985). Statin inhibits the activity of HMGCR and triggers a robust homeostatic feedback response to stabilize the level of cholesterol (Jawaid et al., 2010). Recently, the MVA pathway has been linked to tumorigenesis (Wejde et al., 1992; Clendening et al., 2010; Karlic et al., 2015; Pandyra et al., 2015). Accordingly, statin has been considered as an anticancer agent (Gutt et al., 2010; Nam et al., 2014; Warita et al., 2014). However, the mechanisms to activate the MVA pathway in cancer are not fully understood.

The transformation of normal cells to cancer cells requires a wide variety of molecular alterations. Cells are fully transformed to the neoplastic stage only when they acquire the capability to survive, proliferate, and disseminate. A previous study has illustrated unique metabolic features of the fully transformed cells (Lu et al., 2010), but little attention has been paid to the metabolic pathways that govern the early steps of cell transformation from preneoplastic lesions to a malignant neoplasm.

Primary cilia are microtubule-based organelles that originate from the mother centrosome and protrude into the extracellular environment. As signaling centers, primary cilia coordinate a series of signal transduction pathways, including Hedgehog and Wnt signaling, all of which are important for normal development and cause severe disorders or diseases (now commonly referred to as ciliopathies) when dis-

Correspondence to Dong Xie: dxie@sibs.ac.cn; Xue-Li Zhang: lejing1996@aliyun.com

The Rockefeller University Press
J. Exp. Med. 2018 Vol. 215 No. 1 177–195
https://doi.org/10.1084/jem.20170399

turbed (Praetorius et al., 2004; Rohatgi et al., 2007; Schneider et al., 2010; Lancaster et al., 2011; Pal and Mukhopadhyay, 2015), highlighting the physiological and pathological roles of primary cilia.

Dysregulation of ciliogenesis is observed in cancer. Primary cilia have been shown to mediate or suppress Hedgehog pathway–dependent tumorigenesis in human basal cell carcinoma and medulloblastoma, suggesting the roles of primary cilia in the tumorigenesis (Han et al., 2009). In addition, disrupted ciliogenesis has been found in pancreatic intraepithelial neoplasia (PanIN), a precursor of invasive pancreatic ductal adenocarcinoma (PDAC), indicating that cilia loss is an early oncogenic event and might control the initial steps of malignant transformation (Seeley et al., 2009). Moreover, cilia assembly regulates autophagy and vice versa (Pampliega et al., 2013; Tang et al., 2013), and activation of the autophagy–lysosome pathway drives metabolic reprogramming in PDAC (Perera et al., 2015), indicating potential regulation of cancer metabolism by cilia. Based on these associations, it is reasonable that cilia might be involved in tumorigenesis by modulating cell metabolism. In this study, we dissect the biological functions of cilia during the malignant transformation of normal cells and explore the underlying mechanism.

RESULTS

Malignant transformation leads to loss of primary cilia

To study the relationship between primary cilia and tumorigenesis, primary cilia were examined using immunofluorescence. Normal MEF (mouse fibroblast), NIH3T3 (mouse fibroblast), Bease-2B (human lung), IOSE80 (human ovary), and HPDE6C7 (human pancreas) cells retained primary cilia with axonemes originating from centrosomes and protruding from the cells' basal bodies. However, ciliogenesis was abnormal in 4T1 (mouse breast), Hepa1-6 (mouse liver), A549 (human lung), Ovca429 (human ovary), and Capan-1 (human pancreas) cancer cells (Fig. 1 A).

Next, the abundance and distribution of primary cilia in normal pancreatic tissues, PanIN, and PDAC tissues were determined. The presentative staining images of primary cilium in normal and cancer tissues are shown in Fig. 1 B. The primary cilia in normal pancreatic tissues often extended toward the lumen. The statistical analysis showed that the majority of PanIN tissues and nearly 100% of PDAC tissues were devoid of primary cilia (Fig. 1 C). These findings suggest that the absence of primary cilia might be a highly conserved feature of malignancies.

To study the causal relationship between cilia loss and malignant transformation, NIH3T3 cells were transformed using the oncogenes E1A and H-Ras and selected based on anchorage-independent growth on soft agar (Fig. S1 A). Three E1A–H-Ras–overexpressing clones showed advantages in colony formation in liquid culture, anchorage-independent growth on soft agar, and focus formation, indicating the malignant transformation of these cells (Fig. 1 D). Strikingly, ciliogenesis appeared to be disrupted in these transformed cells (Fig. 1 D). Moreover, the malignancy of individual clones, as measured by the number of colonies formed on soft agar, was negatively correlated with the abundance of cilia (Fig. 1 D). Next, we investigated whether the transformation of normal pancreatic cells (HPDE6C7) induced cilia loss based on the observations that cilia were lost during the progression of PDAC as shown in Fig. 1 (B and C). Similarly, the malignant transformation of HPDE6C7 by K-Ras^{V12} led to cilia loss and growth advantage in both liquid culture and soft agar (Fig. 1 E). These observations indicate that malignant transformation induces cilia loss.

The inactivation of VHL through mutation frequently leads to cilia loss, cyst development, and neuroendocrine tumorigenesis (Lutz and Burk, 2006; Thoma et al., 2007). Decreased levels of the Vhl protein were found in transformed cells (Fig. S1 B). Importantly, the large T antigen (LT)–transformed MEFs showed reduced cilia length and arrested ciliogenesis in 25% of the cells, and ectopic expression of Vhl almost fully restored the ciliogenesis defect in these transformed cells (Fig. S1, C and D). Accordingly, the up-regulation of Vhl-rescued ciliogenesis in E1A–H-Ras–transformed NIH3T3 cells (Fig. S1, E and F). Collectively, these findings suggest that malignant transformation leads to the loss of primary cilia, possibly by decreasing Vhl protein levels.

Disruption of ciliogenesis sensitizes cells to oncogene-induced transformation

Next, we investigated the biological functions of cilia during the malignant transformation by knocking down Tg737 (also known as intraflagellar transport 88 [Ift88]) and Kif3a (a subunit of the kinesin-II complex), two essential components for cilia, in MEFs and HPDE6C7 cells (Fig. 2 A and Fig. S1 G). Although inhibition of ciliogenesis promoted the growth of MEFs and HPDE6C7 cells (Fig. 2 B), cilia loss promoted neither the anchorage-independent growth of these cells on soft agar nor tumorigenesis in nude mice (Fig. S1 H), suggesting that the disruption of ciliogenesis alone was insufficient to transform the MEFs. However, disrupting ciliogenesis by knocking down Tg737 or KIF3A potentiated the transformation of HPDE6C7 cells by K-Ras^{V12}, which was demonstrated in the anchorage-independent growth assay (Fig. 2 C). Moreover, inhibition of ciliogenesis potentiated the transformation of NIH3T3 cells by WT Ras, as assessed based on tumor formation in nude mice (Fig. 2, D and F; and Fig. S1 I). Accordingly, the disruption of ciliogenesis significantly enhanced tumor formation from LT-transformed NIH3T3 cells and Ras^{V12}-transformed MEFs (Fig. S1, J and K). In summary, these observations indicate that the inhibition of ciliogenesis sensitizes normal cells to oncogene-driven malignant transformation.

Disruption of ciliogenesis activates the MVA pathway

To explore the underlying molecular mechanisms, a microarray analysis was performed to identify the genes regulated by the primary cilia by overlapping the differentially ex-

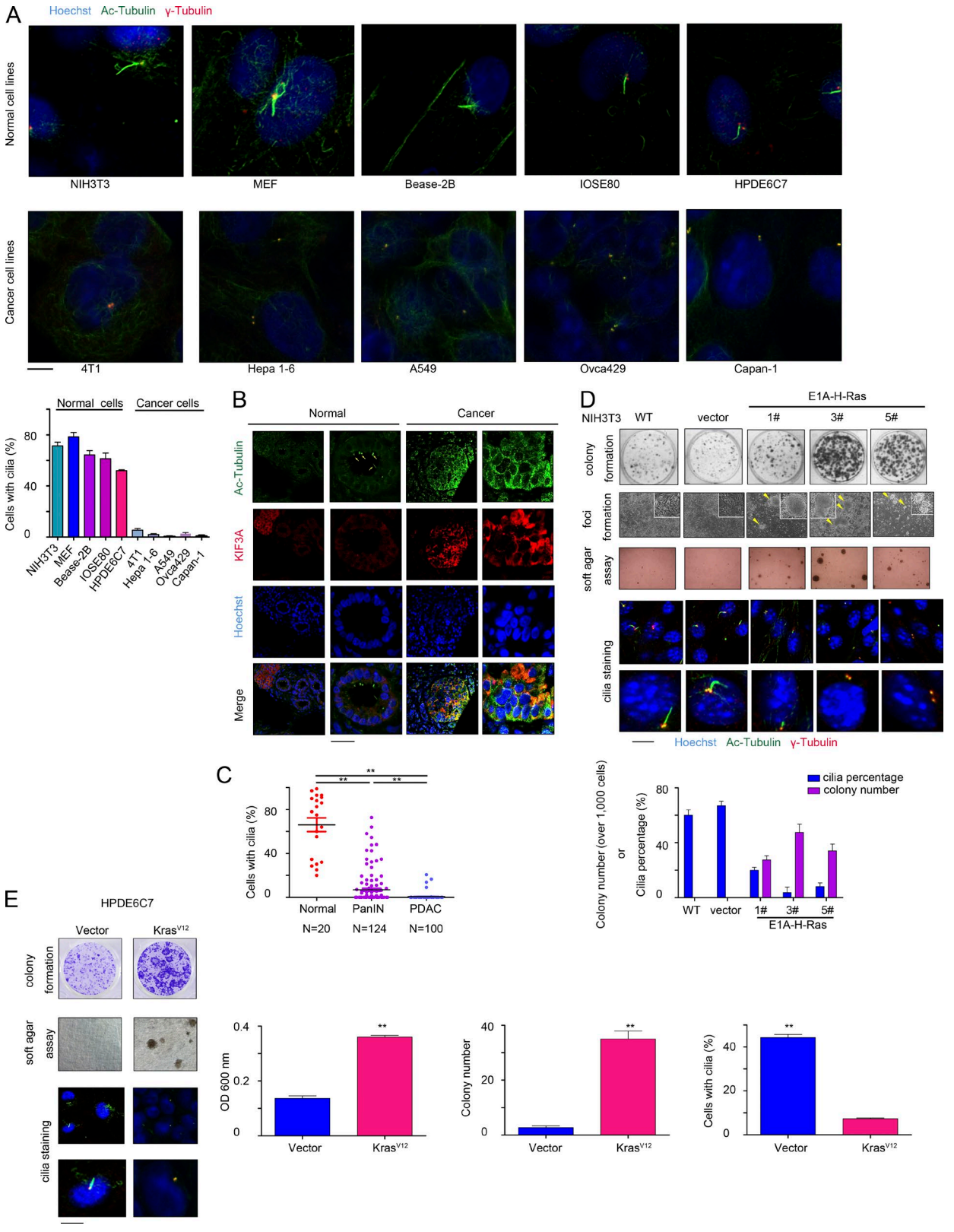

Figure 1. **The cilia are lost in cancer cells. (A)** Cilia staining in normal cells and cancer cells. Acetylated tubulin was used to label cilia, γ-tubulin to label the centrosome, and Hoechst to label the nucleus. The mouse-derived normal cells (NIH3T3 and MEF), the human normal lung bronchus cells (Bease-2B), the normal pancreatic cells (HPDE6C7), and the normal ovarian cells (IOSE80) had cilia, whereas the mouse-derived cancer cells (4T1 and Hepa1-6), human

pressed genes regulated by Kif3a or Tg737 in MEFs. 1,026 Kif3a-related genes and 484 Tg737-related genes were identified, among which 110 genes overlapped (78 down-regulated genes and 32 up-regulated genes) in Kif3a or Tg737 knockdown cells (Fig. 3, A and B). These differentially expressed genes could be classified into 13 categories according to their various cellular functions (Fig. 3 C and Table S1). Interestingly, ∼20% of the differentially expressed genes were enzymes involved in cell metabolism, indicating that the disruption of ciliogenesis might reprogram metabolic pathways.

These differentially expressed enzymes were involved in multiple metabolic pathways. Surprisingly, ∼50% of the differentially expressed enzymes were specific to cholesterol biosynthesis (MVA pathway), and their expression was significantly increased after the disruption of primary cilia formation (Fig. 3 C), which was confirmed by quantitative PCR (Fig. S2 A). Interestingly, cilia loss and increased expression of MVA enzymes in LT-transformed MEF cells were observed (Fig. S1 C and Fig. S2 B). In addition, knocking down the expression of Tg737 in MEFs up-regulated the levels of the Hmgcr protein, which is the rate-limiting enzyme in the MVA pathway (Fig. S2 C). Moreover, knocking down the expression of KIF3A and Tg737 up-regulated the mRNA levels of MVA enzymes and the HMGCR protein levels in human normal pancreatic cells (HPDE6C7; Fig. 3 D). The AURA-HEF1 cascade played a pivotal role in the degradation of cilium (Pugacheva et al., 2007). Mining the Gene Expression Profiling Interactive Analysis database revealed that the expression of HFE1 and AURA positively correlated with the expression of MVA enzymes in pancreatic cancer, adrenocortical carcinoma, and ovarian serous cystadenocarcinoma, respectively (Table S2 and Table S3). These findings suggested that the up-regulation of MVA enzymes by cilia loss was not cell type specific.

However, overexpressing the siRNA-resistant Kif3a construct rescued the ciliogenesis deficiency caused by Kif3a knockdown and down-regulated the expression of the MVA enzymes (Fig. S2 D), confirming the activation of this specific metabolic pathway after cilia loss. Moreover, depletion of *Tg737* in pancreatic tissues increased the body weight of the mice and the ratio between pancreas weight and body weight, induced the formation of cysts in pancreatic tissues, and increased the mRNA levels of several enzymes in the MVA pathway as well as levels of Hmgcr protein (Fig. 3, E and F; and Fig. S2, E and F). Collectively, these findings indicate that the inhibition of ciliogenesis activates the MVA pathway.

Disruption of ciliogenesis sensitizes cells to oncogene-induced transformation by activating the MVA pathway

Next, we investigated the roles of the MVA pathway in malignant transformations. Statin treatment significantly impaired the increased colony formation ability of Kif3a or Tg737 knockdown HPDE6C7 cells and MEFs (Fig. 4 A and Fig. S2 G), suggesting that cells in which ciliogenesis is inhibited are more dependent on the MVA pathway for survival and growth. Consistent with this notion, the half-maximal inhibitory concentration of statin in MEFs with disrupted ciliogenesis was much lower than in control cells (Fig. 4 B).

Farnesyl diphosphate (FPP) and geranylgeranyl pyrophosphate (GGPP) are two downstream metabolic intermediates of the HMGCR enzyme. Both FPP and GGPP, but not cholesterol, overcame the inhibitory effects of statin on colony formation in HPDE6C7 cells and MEFs with disrupted ciliogenesis (Fig. 4 C and Fig. S2, H and I). Moreover, as shown in Fig. 2 (C, E, and F), statin effectively inhibited the tumorigenicity of HPDE6C7 and NIH3T3 cells with disrupted ciliogenesis in soft agar and a xenograft mouse model, respectively. These results demonstrate that the activation of the MVA pathway after the disruption of ciliogenesis contributed to cell transformation in vivo.

The metabolic intermediates of the MVA pathway are responsible for the full activation of the Ras protein (Cuthbert and Lipsky, 1995). Next, we examined whether the disruption of ciliogenesis regulated Ras–Erk signaling. A glutathione *S*-transferase (GST)–Ras-binding domain (RBD) pull-down and immunoblot assays showed that knocking down either Kif3a or Tg737 potentiated the activation of Ras (Fig. 4 D) and promoted the phosphorylation of Erk (Fig. 4 E) in epidermal growth factor (EGF)–treated MEFs and HPDE6C7 cells, indicating that Ras–Erk signaling was enhanced by blocking ciliogenesis in these cells. Consistent with the previous study, statin exposure decreased Erk phosphorylation in the control cells (Wu et al., 2004). However, the enhancement of Erk phosphorylation in MEFs after the knockdown of Tg373 was inhibited by statin and rescued by FPP (Fig. 4 F), suggesting that the disruption of ciliogenesis boosts Ras–Erk signaling by increasing the activity of the MVA pathway. Together, these results indicate that the activation of the MVA pathway after cilia loss may mediate oncogene-induced transformation by activating Ras–Erk signaling.

lung cancer cells (A549), human ovarian cancer cells (Ovca429), and human pancreatic cancer cells (Capan-1) lost cilia. Quantification was performed to analyze the percentage of ciliated cells (bottom). **(B)** Cilia staining in nonneoplastic ducts and PDAC. Hoechst was used to label the nucleus. The arrows indicate the primary cilium. **(C)** Percentage of ciliated cells in normal pancreatic ducts, PanINs, and PDAC tissues. The cilium staining was performed in the formalin-fixed and paraffin-embedded pancreatic tissues using acetylated tubulin and Kif3a as the marker. **(D)** Colony formation assay, focus formation assay, soft agar assay, and cilia staining of transformed NIH3T3 cells. Quantification for the results is shown below. **(E)** Colony formation assay, soft agar assay, and cilia staining of Ras^{V12}-transformed HPDE6C7 cells. Bars: (A, D, and E) 5 µm; (B) 40 µm. **, $P < 0.01$. The data are presented as the mean ± SEM. Representative plots are of at least two independent experiments. Student's *t* test was performed.

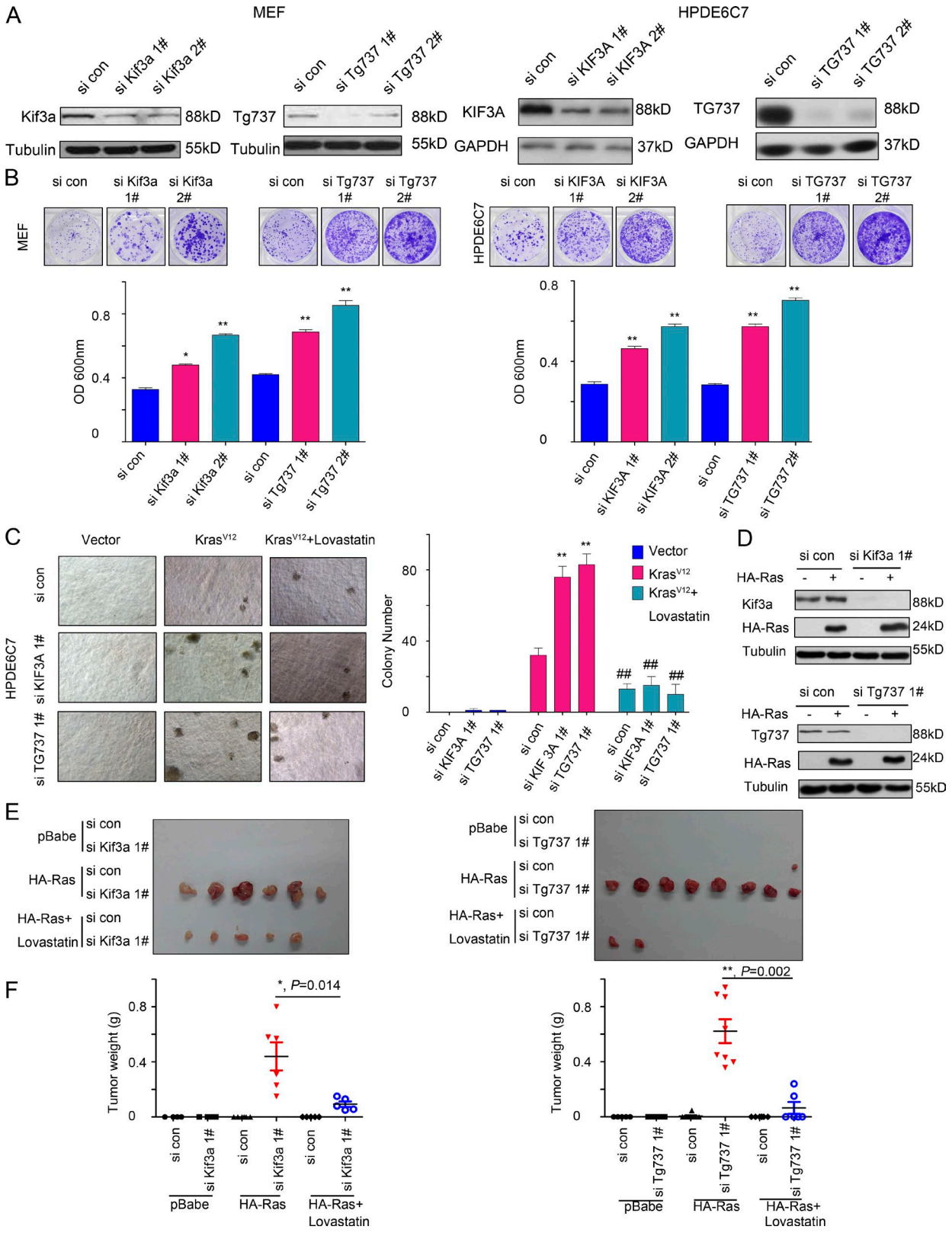

Figure 2. **Disruption of ciliogenesis sensitizes cells to malignant transformation. (A)** Knocking down the expression of Tg737 and Kif3a in MEFs and HPDE6C7 cells. **(B)** Down-regulation of Tg737 and Kif3a promoted the growth of MEFs and HPDE6C7 cells in the crystal violet assay. **(C)** Knocking down the expression of Tg737 and KIF3A promoted the transformation of HPDE6C7 cells driven by Ras^{V12} in the soft agar assay. ##, $P < 0.01$. **(D)** Overexpression of

Activation of β-catenin–T cell factor (TCF) signaling after the disruption of ciliogenesis synchronizes with SREBP2 and promotes the expression of enzymes involved in the MVA pathway

Next, how the MVA pathway was activated in cells with disrupted ciliogenesis was investigated. Inhibition of ciliogenesis leads to activation of β-catenin–TCF signaling (Fig. S3 A; Lancaster et al., 2011). However, it remained unknown whether β-catenin–TCF signaling could potentiate the activity of the MVA pathway. MEFs were treated with 25 mM lithium (LiCl; inhibitor of GSK3-β) to stimulate β-catenin–TCF signaling, and multiple enzymes involved in the MVA pathway (especially Hmgcs1, Hmgcr, Idi1, and Cyp51), as well as the known target gene *Axin*, were found to be up-regulated (Fig. 5 A). LiCl treatment did not induce the cleavage of SREBP2, suggesting the up-regulation of MVA enzymes by LiCl treatment independent of the activation of SREBP2 (Fig. S3 B). Moreover, the response of these genes' expression to LiCl was comparable to that of statin (Fig. S3 C).

Similarly, overexpression of β-catenin in MEFs up-regulated the mRNA levels of Hmgcs1, Hmgcr, Idi1, and Cyp51 (Fig. S3 D), whereas knocking down the expression of β-catenin inhibited the expression of these enzymes (Fig. 5 B). These observations indicate that β-catenin–TCF signaling regulates the expression of enzymes involved in the MVA pathway. Furthermore, several β-catenin–TCF–binding elements (TBEs) were identified in the promoters of *Hmgcs1*, *Hmgcr*, *Idi1*, and *Cyp51*, and overexpression of β-catenin significantly activated these promoters in luciferase assays (Fig. S3 E). It has been well studied that Hedgehog signaling is regulated by the primary cilium. However, Gli1 did not activate the promoters of *Hmgcs1*, *Hmgcr*, *Idi1*, and *Cyp51* (Fig. S3 E). Moreover, overexpression of Gli1 in HPDE6C7 cells dramatically elevated the expression of its target gene (FOXM1) but not MVA enzymes (Fig. S3 F). In addition, no positive correlation between the expression of Gli1 and HMGCR in the pancreatic cancer tissues was observed (Fig. S3 G). Promoters with mutated TBE sequences were not activated by β-catenin (Fig. S3 H), and chromatin immunoprecipitation (ChIP) assays demonstrated that β-catenin formed DNA–protein complexes at the promoters of *HMGCS*, *HMGCR*, *IDI1*, *CYP51*, and mouse *Hmgcr* (Fig. 5 C), suggesting that β-catenin signaling directly regulates Hmgcs1, Hmgcr, Idi1, and Cyp51 transcription.

Next, the second TBE (TBE2) in the endogenous HMGCR promoter region was edited by dCas9/small guide RNA (sgRNA) to block its binding with the β-catenin–TCF complex. As shown in Fig. 5 (D and E), overexpression of β-catenin in HPDE6C7 cells (WT HMGCR promoter) induced a higher mRNA level and protein level of HMGCR compared with that of HPDE6C7 cells (dCas9-edited HMGCR promoter). Consistently, the mRNA level of HMGCR in HPDE6C7 (with WT HMGCR promoter) was induced in a time window upon the stimulation of LiCl and statin. However, no response or a weaker response of HMGCR mRNA levels was observed in cells with dCas9-edited HMGCR promoter (Fig. S3, I and J). Moreover, dCas9-edited TBE2 inhibited the binding of β-catenin to HMGCR promoter (Fig. 5 F). In addition, editing TBE2 in HMGCR promoter with the dCas9 system did not affect the expression of c-Jun in HPDE6C7 cells upon the treatment of lithium (Fig. S3 K), suggesting the decreased expression of HMGCR in HPDE6C7 cells (with dCas9-edited HMGCR promoter) was not caused by the reduced β-catenin protein level. Collectively, these data clearly demonstrate that β-catenin directly regulates the expression of HMGCR.

We then examined whether β-catenin synchronized with the N terminus of SREBP2 (SREBP2N) to regulate the expression of HMGCR. In the reporter assay, TBE2 mutation (mTBE2) attenuated the activation of HMGCR promoter induced by SREBP2N (Fig. 5 G). Moreover, immunoprecipitation assay and GST pull-down assay demonstrated that β-catenin interacted with SREBP2N (Fig. 5 H). Furthermore, dCas9-mediated editing of TBE2 not only impaired the interaction between SREBP2N and HMGCR promoter (Fig. 5 I), but also blunted the induction of HMGCR by exogenous SREBP2N (Fig. 5 J). In summary, these data suggested that the binding of β-catenin in the TBE2 region up-regulated the expression of HMGR by synchronizing with the N terminus of SREBP2.

In addition, overexpression of dominant-negative β-catenin or ICAT (two negative regulators of β-catenin–TCF signaling) inhibited the increased expression of Hmgcs1, Hmgcr, Idi1, and Cyp51 induced by disrupted ciliogenesis (Fig. 5 K). Moreover, the nuclear localization of β-catenin was well correlated with the up-regulation of Hmgcr in pancreatic tissues of *Tg737* KO mice (Fig. S3 L), further supporting the notion that the inhibition of ciliogenesis up-regulates the expression of enzymes involved in the MVA pathway by activating β-catenin signaling.

Cilia loss and up-regulation of HMGCR in the PanINs driven by $Kras^{G12D}$

$Kras^{G12D}$ induces ductal lesions that recapitulate the full spectrum of human PanIN (Hingorani et al., 2003). Consistently, the higher ratio of pancreas weight to body and more active Ras protein were found in the pancreas of *Pdx-Cre; $Kras^{G12D}$* mice (Fig. S4, A and B). As the mice aged (from 8 mo after birth), PanINs were observed in *Pdx-Cre; $Kras^{G12D}$* mice at an increasing frequency (Fig. S4 C). These observations suggest

HA-Ras and down-regulation of Tg737 and Kif3a in NIH3T3 cells. **(E)** Disruption of ciliogenesis sensitized NIH3T3 cells to transformation by WT Ras, which was inhibited by statin. **(F)** The weight of the tumors in E. Student's *t* test was performed. (E and F) $n = 6$ for the Kif3a group and $n = 8$ for the Tg737 group. *, $P < 0.05$; **, $P < 0.01$. The data are presented as the mean ± SEM. Representative plots are of at least two independent experiments. si con, siRNA control.

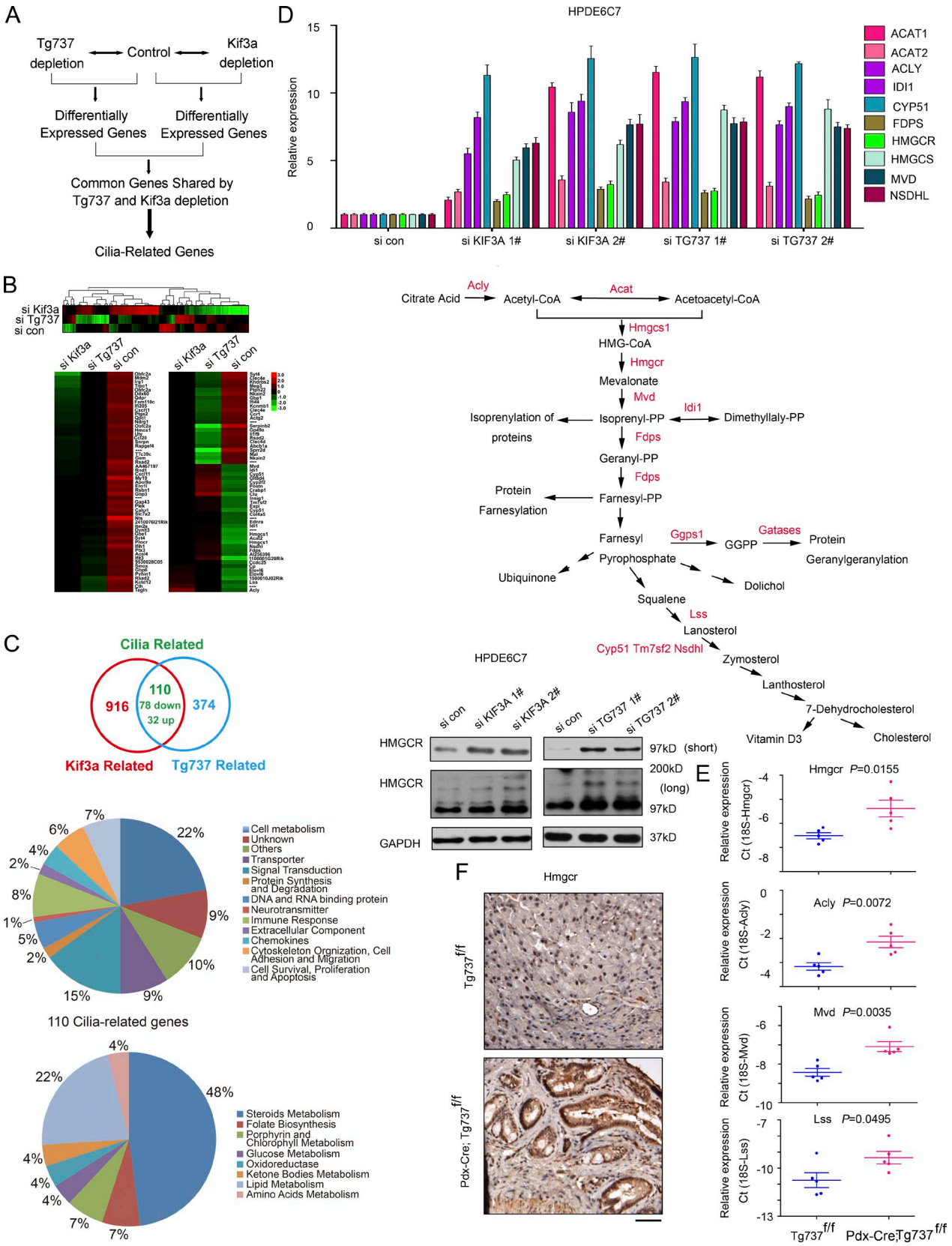
A
Tg737 depletion
Control
Kif3a depletion
Differentially Expressed Genes
Differentially Expressed Genes
Common Genes Shared by Tg737 and Kif3a depletion
Cilia-Related Genes
B
si Kif3a
si Tg737
si con
C
Cilia Related
916
110
78 down
32 up
374
Kif3a Related
Tg737 Related
110 Cilia-related genes
Cell metabolism
Unknown
Others
Transporter
Signal Transduction
Protein Synthesis and Degradation
DNA and RNA binding protein
Neurotransmitter
Immune Response
Extracellular Component
Chemokines
Cytoskeleton Orgnization, Cell Adhesion and Migration
Cell Survival, Proliferation and Apoptosis
Steroids Metabolism
Folate Biosynthesis
Porphyrin and Chlorophyll Metabolism
Glucose Metabolism
Oxidoreductase
Ketone Bodies Metabolism
Lipid Metabolism
Amino Acids Metabolism
D
HPDE6C7
Relative expression
si con
si KIF3A 1#
si KIF3A 2#
si TG737 1#
si TG737 2#
ACAT1
ACAT2
ACLY
IDI1
CYP51
FDPS
HMGCR
HMGCS
MVD
NSDHL
Acly
Acat
Citrate Acid
Acetyl-CoA
Acetoacetyl-CoA
Hmgcs1
HMG-CoA
Hmgcr
Mevalonate
Mvd
Idi1
Isoprenylation of proteins
Isoprenyl-PP
Dimethyllaly-PP
Fdps
Geranyl-PP
Fdps
Protein Farnesylation
Farnesyl-PP
Farnesyl
Ggps1
GGPP
Gatases
Protein Geranylgeranylation
Ubiquinone
Pyrophosphate
Dolichol
Squalene
Lss
Lanosterol
Cyp51 Tm7sf2 Nsdhl
Zymosterol
Lanthosterol
7-Dehydrocholesterol
Vitamin D3
Cholesterol
HPDE6C7
si con
si KIF3A 1#
si KIF3A 2#
si con
si TG737 1#
si TG737 2#
HMGCR
97kD (short)
HMGCR
200kD (long)
97kD
GAPDH
37kD
E
Hmgcr P=0.0155
Acly P=0.0072
Mvd P=0.0035
Lss P=0.0495
Relative expression
Ct (18S-Hmgcr)
Ct (18S-Acly)
Ct (18S-Mvd)
Ct (18S-Lss)
Tg737f/f
Pdx-Cre;Tg737f/f
F
Hmgcr
Tg737f/f
Pdx-Cre; Tg737f/f

that the conditional $Kras^{G12D}$ allele efficiently recombined in the pancreas of *Pdx-Cre; $Kras^{G12D}$* mice.

To investigate the relationship between ciliogenesis and the progression of $Kras^{G12D}$-induced cell transformation, we first measured ciliogenesis in the pancreas of *Pdx-Cre; $Kras^{G12D}$* mice at different ages and observed a dramatic reduction in cilia formation from ∼70 to 15% at the age of 8 mo when numerous PanIN lesions were observed (Fig. 6 A and Fig. S4 D). The expression of enzymes involved in the MVA pathway, such as Hmgcr, was up-regulated (Fig. 6 B and Fig. S4 E). In addition, cilia loss and up-regulation of Hmgcr and Cyp51 in PanIN tissues were simultaneously observed through immunostaining consecutive sections (Fig. 6 C). To assess the correlation between cell transformation and the activities of the β-catenin and MVA pathways, we used mucin 5 (Muc5), a biomarker of PanIN, to evaluate cell transformation and examined the expression levels of Muc5, Hmgcr, and β-catenin in *Pdx-Cre; $Kras^{G12D}$* mice. As the frequency of PanIN formation increased in the pancreas of *Pdx-Cre; $Kras^{G12D}$* mice aged 2–13 mo, simultaneous up-regulation of Muc5 and Hmgcr expression and β-catenin nuclear localization were detected (Fig. 6 D and Fig. S4, F and G). The expression levels of Muc5, Hmgcr, and β-catenin were positively correlated (Fig. 6 E), and the level of ciliogenesis was negatively correlated with the expression of Muc5 and nuclear β-catenin (Fig. 6 F). Collectively, these results suggest that there are strong correlations between cilia loss and activation of the β-catenin and MVA pathways during tumorigenesis in the PanIN mouse model.

Cilia loss is correlated with activation of the MVA pathway in human PDAC samples

Next, we sought to examine whether cilia loss led to activation of the MVA pathway in human PDAC samples based on the cilia loss in human PDAC (Fig. 1, B and C). The mRNA level of MVA enzymes was found to be up-regulated in 64 human PDAC samples compared with paired normal tissues (Fig. 7 A). Moreover, cilia loss in human PanIN and PDAC tissues was well correlated with the up-regulation of HMGCR protein levels (Fig. 7 B). In addition, the cytoplasmic accumulation and nuclear localization of β-catenin were positively correlated with the expression of HMGCR in human PDAC samples (Fig. 7 C). These results strongly indicate the clinical significance of cilia loss–mediated β-catenin–MVA signaling during tumor progression in PDAC patients.

To further dissect the role of cilia loss during PDAC tumorigenesis and the therapeutic effects of statin, PanIN formation was examined in 8-mo-old *Pdx-Cre; $Kras^{G12D}$; $Tg737^{loxp/loxp}$* mice and *Pdx-Cre; $Kras^{G12D}$* mice, with and without statin treatment. Compared with *Pdx-Cre; $Kras^{G12D}$* mice, the *Pdx-Cre; $Kras^{G12D}$; $Tg737^{loxp/loxp}$* mice presented more PanINs (Fig. 7, D and E), suggesting that disruption of ciliogenesis promotes PanIN formation in oncogenic $Kras^{G12D}$-driven tumorigenesis. Interestingly, statin administration effectively inhibited PanIN formation, indicating the critical roles of the MVA pathway during tumor progression. Consistent with these observations, the expression of Muc5 was increased in *Pdx-Cre; $Kras^{G12D}$; $Tg737^{loxp/loxp}$* mice and decreased after statin treatment (Fig. 7, D and E). Moreover, the expression of Hmgcr was enhanced in the pancreatic tissues of *Pdx-Cre; $Kras^{G12D}$; $Tg737^{loxp/loxp}$* mice, which might explain the therapeutic effects of statin (Fig. 7 F). Collectively, these results indicate that activation of the MVA pathway after cilia loss promotes PDAC tumorigenesis.

DISCUSSION

Numerous studies show the reprogrammed metabolic pathways in cancer (Gordan et al., 2007; Lu et al., 2010). However, most of these studies were performed using fully transformed cancer cells as models, and the reprogramming of metabolic pathways during the early phase of transformation and its specific contribution to the tumorigenic process remain largely undescribed. In this study, we reveal that the MVA pathway is activated by disrupted ciliogenesis and could accelerate the oncogene-induced transformation of normal cells both in vitro and in vivo (Fig. 7 G). Although cooperation between the MVA pathway and Ras in cell transformation has been reported (Clendening et al., 2010), our study reveals the link between cilia loss, activation of the MVA pathway, and cell transformation.

In this study, shorter cilia or cilia loss was not only observed in well-established cancer cell lines, but was also gradually observed in normal pancreatic cells and NIH3T3 cells during the transformation process, which is consistent with previous reports of ciliogenesis defects in human glioma, breast, and kidney cancer (Han et al., 2009; Seeger-Nukpezah et al., 2013). Moreover, cilia loss was detected in a mouse

Figure 3. **Disrupting ciliogenesis activates the MVA pathway. (A)** Strategy to identify cilia-related genes by microarray analysis. **(B)** Venn diagram showing the relationship between Tg737-related genes, Kif3a-related genes, and cilia-related genes. Heat map representation of unsupervised hierarchical clustering and a heat map showing 110 cilia-related genes (bottom). The shades of red and green represent increases and decreases in the expression of the corresponding genes, respectively. **(C)** Pathway analysis for the 110 cilia-related genes. Approximately 20% of the genes were enzymes involved in metabolism (top), in which ∼50% of the genes were involved in steroid metabolism (bottom). **(D)** Knocking down Tg737 or KIF3A increased the mRNA levels of enzymes in the MVA pathway and the protein level of HMGCR in HPDE6C7 cells. The short exposure revealed the monomer of HMGCR (97 kD), and the long exposure revealed the dimer of HMGCR (∼200 kD). Most of the HMGCR existed as monomers. **(E and F)** Disrupting ciliogenesis in pancreatic tissues of Tg7373 KO mice increased the mRNA level of MVA pathway–related genes (n = 5 for each group) as well as the level of Hmgcr protein in the immunohistochemistry assay. Bar, 40 µm. Student's t test was performed. The data are presented as the mean ± SEM. Representative data are of at least two independent experiments. si con, siRNA control.

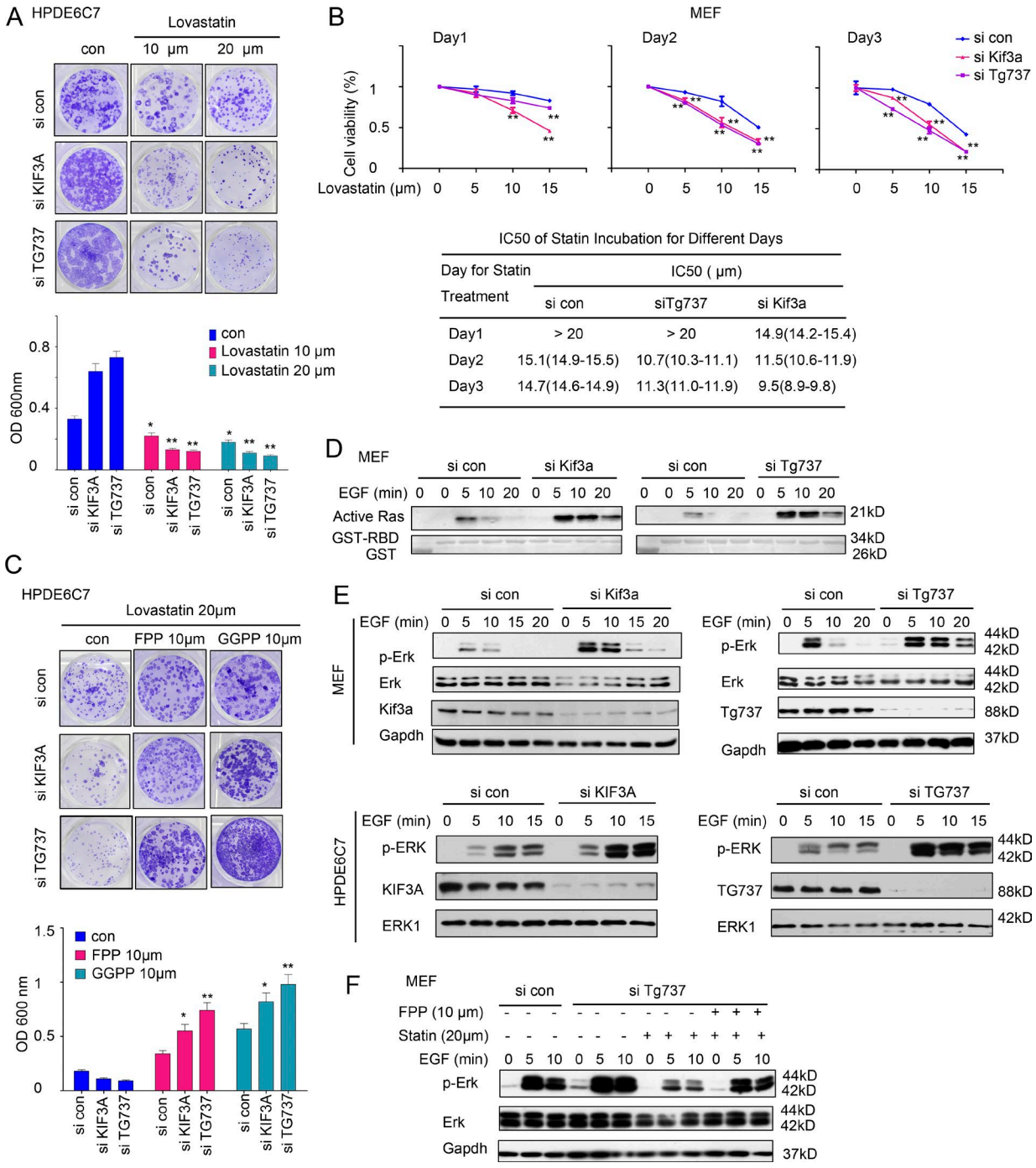

Figure 4. **Activation of the MVA pathway promotes cell growth. (A)** Disruption of ciliogenesis sensitized the HPDE6C7 cells to the inhibition of statin in the colony formation assay. **(B)** Control MEF cells and cells depleted of Tg737 or Kif3a were treated with statin. The survival of the cells was measured. The table shows the half-maximal inhibitory concentration (IC50) of statin. **(C)** FPP and GGPP rescued the inhibitory effects of statin on the HPDE6C7 cells. **(D and E)** Disrupting ciliogenesis by knocking down Kif3a and Tg737 promoted the activation of Ras–ERK signaling. Disrupting ciliogenesis promoted the activation of Ras in MEFs in the GST pull-down assay (D) and the phosphorylation of ERK in MEFs and HPDE6C7 cells (E). **(F)** Statin inhibited EGF-induced ERK phosphorylation, which was rescued by FPP. Cells were treated with 20 μM statin (with or without 10 μM FPP) for 48 h, and then the cells were treated with 10 ng/ml EGF. *, $P < 0.05$; **, $P < 0.01$. The data are presented as the mean ± SEM. Representative data are of at least two independent experiments. si con, siRNA control. Student's *t* test was performed.

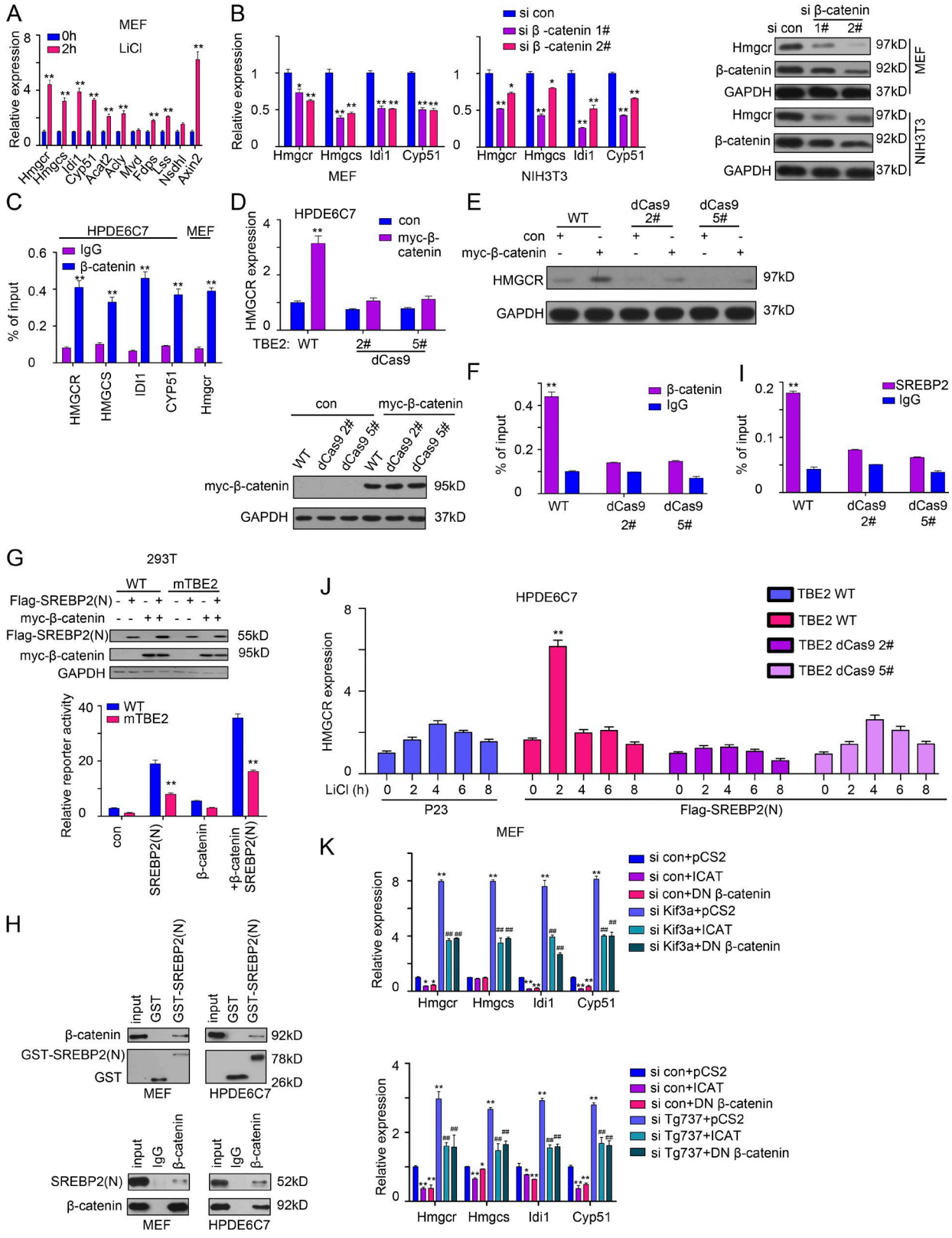

Figure 5. **Disrupting ciliogenesis activates the MVA pathway by positively regulating β-catenin–TCF signaling. (A)** Lithium elevated the mRNA level of enzymes in the MVA pathway. MEF cells were treated with 25 mM LiCl, and the mRNA levels of MVA enzymes were examined using real-time PCR. **(B)** Knocking down the expression of β-catenin reduced the level of the mRNA levels of Hmgcs, Hmgcr, Idi1, and Cyp51 proteins in MEFs and NIH3T3 cells.

model of PanIN (a precursor of PDAC), and the percentage of cells with cilia was inversely correlated with PanIN number and Muc5 expression (a biomarker of PanIN), suggesting that cilia loss is an early event during malignant transformation. In fact, in each transformed NIH3T3 clone that we established, a small fraction of cells possessed primary cilia. However, the more cilia the cells maintained, the less malignant their phenotype was. Therefore, in most cases, cilia loss is prevalent during tumor development and is positively correlated with tumor malignancy, suggesting that cilia could serve as a potential biomarker for diagnosis and prediction.

Although the disruption of ciliogenesis in cancer is well documented, the causal relationship between cilia loss and tumorigenesis is poorly understood. To address this issue, cilia were destroyed by inhibiting the expression of *Tg737* or *Kif3a*, two common genes involved in cilia assembly. As expected, the disruption of ciliogenesis did not induce tumor formation, which is consistent with previous observations that ciliopathies do not predispose patients to cancer, except in a limited number of cases (Michaud and Yoder, 2006). In addition, although *Tg737* or *Kif3a* conditional KO mice displayed cyst formation, no tumors were observed. However, the disruption of ciliogenesis sensitized normal cells to transformation induced by the oncogene Ras or LT. These results indicate that cilia might protect cells from malignant transformation, and cells with disrupted ciliogenesis might become a transformation-prone subpopulation within a tissue.

In this study, cilia loss significantly increased the expression of enzymes for lipid (such as Acly) and cholesterol synthesis (enzymes involved in the MVA pathway), which might explain the observation that obesity is a common manifestation of human ciliopathies (Mok et al., 2010; Acs et al., 2015). Furthermore, a positive correlation between the activation of the MVA pathway and cilia loss was detected in a PanIN mouse model and human PDAC samples. These findings further supported our notion that activation of the MVA pathway after the disruption of ciliogenesis sensitizes cells to transformation.

Regarding the transformation of normal cells, the reprogramming of metabolic pathways might be important for the initiation of tumorigenesis in the execrable tumor microenvironment (Hanahan and Weinberg, 2011). It is well known that angiogenesis is not involved in the very early stage of tumorigenesis, which deprives the initially transformed cells of sufficient nutrients, including glucose, lipid, cholesterol, and oxygen (Hanahan and Weinberg, 2011). Therefore, only a small fraction of cells survive and form clones by gaining oncogenic mutations and bypassing the metabolic obstacle while the remainder of cells may succumb to senescence and apoptosis. Cilia loss activates the MVA pathway and increases cholesterol synthesis, which might initially help transformed cells to adapt to metabolic stress and enhance the efficiency of transformation.

In addition to the end product cholesterol, the MVA pathway produces many nonsterol isoprenoids, such as FPP and GGPP, which mediate protein prenylation via the covalent addition of isoprenoids, resulting in the attachment of hydrophobic prenyl groups that anchor the substrates to intracellular membranes. Small G proteins, such as Ras, Rho, and Rac, which are crucial cancer-related genes whose functions are greatly dependent on their membrane localization, are among the most important substrates of FPP and GGPP (Xu et al., 2015). In this study, FPP and GGPP were found to rescue the inhibitory effect of statin, which further demonstrates the importance of the MVA pathway in the malignant transformation of cells without cilia. Thus, activation of the MVA pathway after cilia loss might enhance the production of FPP and GGPP to activate oncogenic small guanosine triphosphatases, which could be blocked by statin treatment, resulting in impaired malignant transformation.

Statin has been considered for application in the prevention and treatment of cancer (Bardou et al., 2010; D'Amico, 2010; Gutt et al., 2010). In support of this proposition, we found that statin treatment could effectively reverse the oncogenic phenotype induced by the disruption of ciliogenesis. Moreover, statin effectively impaired cellular transformation in vitro and tumor development in the PDAC mouse model. These observations suggest that cells with disrupted ciliogenesis are more dependent on the MVA pathway for survival and, thus, are more sensitive to statin treatment. Consistent

(C) ChIP assay using β-catenin antibody to examine the interaction between β-catenin and promoters of HMGCS, HMGCR, IDI1, CYP51, and mouse Hmgcr. Real-time PCR was performed. **(D and E)** dCas9-edited HMGCR promoter (dCas9 2 and dCas9 5) impaired the expression of HMGCR mRNA (D) and protein level (E) induced by overexpressing β-catenin. The TBE2 in the endogenous HMGCR promoter of HPDE6C7 cells was edited by the dCas9 system. The details are described in Materials and methods. **(F)** dCas9-edited HMGCR promoter (dCas9 2 and dCas9 5) impaired its binding with β-catenin. The complex of β-catenin and DNA was immunoprecipitated using β-catenin antibody. Real-time PCR was performed to examine the TBE2 of HMGCR promoter. **(G)** Mutation of TBE2 (mTBE2) impaired the activation of HMGCR promoter synchronized by β-catenin and SREBP2N. The Flag-tagged N terminus of SREBP2 (Flag-SREBP2N) plasmid and the myc-tagged β-catenin (myc–β-catenin) plasmid were transfected with human HMGCR promoter (WT) or the HMGCR promoter with TBE2 mutation (mTBE2) into 293T cells. The activities of the reporters were measured. **(H)** GST pull-down assay and immunoprecipitation assay were performed to show the interaction between β-catenin and SREBP2N. **(I)** dCas9-edited HMGCR promoter (dCas9 2 and dCas9 5) impaired the interaction between SREBP2 and TBE2 in the HMGCR promoter. The complex of SREBP2 and DNA was immunoprecipitated using SREBP2 antibody. Real-time PCR was performed to examine the TBE2 of HMGCR promoter. **(J)** dCas9-edited TBE2 in the HMGCR promoter impaired the increased HMGCR mRNA level synchronized by LiCl and SREBP2N. **(K)** ICAT and dominant-negative β-catenin impaired the induction of Hmgcs1, Hmgcr, Cyp51, and Idi1 after disrupted ciliogenesis. Student's *t* test was performed. ##, $P < 0.01$; *, $P < 0.05$; **, $P < 0.01$. The data are presented as the mean ± SEM. Representative data are of at least two independent experiments. si con, siRNA control.

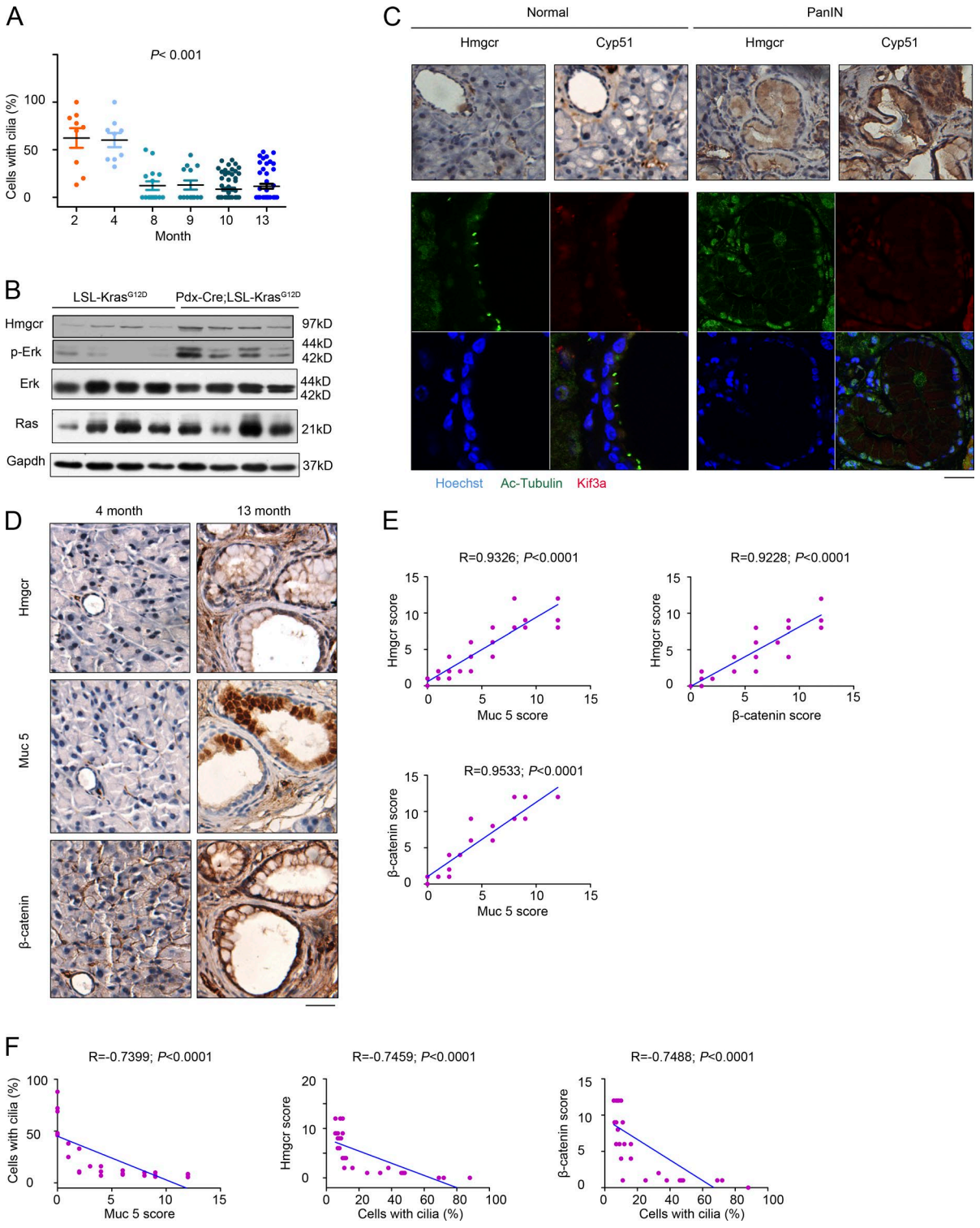

Figure 6. **Disruption of ciliogenesis is correlated with the activation of the MVA pathway in a PDAC mouse model. (A)** Disruption of ciliogenesis in the pancreatic tissues of *Pdx-Cre; Kras*^{G12D} mice. The pancreatic tissues of *Pdx-Cre; Kras*^{G12D} mice were harvested at the indicated time points. The percentage of ciliated cells was examined by immunostaining and quantified (n = 9–24 for each time point). ANOVA was performed. **(B and C)** Up-regulation of Hmgcr and CYP51 and disruption of ciliogenesis in the pancreatic tissues of 8-mo-old *Pdx-Cre; Kras*^{G12D} mice (n = 4 for each group). The pancreatic tissues were isolated from 8-mo-old *Pdx-Cre; Kras*^{G12D} mice and their control littermates, the levels of the indicated proteins were examined by Western blot (B) or immunohistochemistry (C), and the cilia were examined using immunostaining**. (D)** Expression of Muc5, β-catenin, and Hmgcr in the *Pdx-Cre; Kras*^{G12D} mice at the indicated time points. (C and D) Bars, 40 µm. **(E)** The correlations between the expression of Hmgcr, β-catenin, and Muc5 for each individual

with this finding, it has been reported that tumor cells are more sensitive to statin treatment than normal cells (Wong et al., 2007). Because most tumor cells display deficient ciliogenesis, it is tempting to speculate that the antitumorigenic effects of statins are required to reduce the activity of the MVA pathway induced by the loss of cilia. It has been reported that MVA pathway interplays with several signal pathways in the tumorigenesis (Mullen et al., 2016). Therefore, these findings support the potential application of statin in clinical settings for chemoprevention and, possibly, cancer therapy.

Another important finding of this study is that the MVA pathway is regulated by β-catenin–TCF signaling, highlighting the important roles of this signaling pathway in regulating cancer metabolism. Several enzymes in the MVA pathway, including Hmgcr, were demonstrated to be direct target genes of β-catenin–TCF signaling.

Moreover, β-catenin was found to form a complex with SREBP2 on the promoters of the genes involved in the MVA pathway. Consistently, SREBP signaling has been reported to integrate with the Wnt–β-catenin and glucocorticoid receptor signaling pathways during perinatal lung maturation (Bridges et al., 2014), suggesting cross talk between β-catenin signaling and SREBP proteins. Consistent with our observations, several oncogenic proteins (for example, mutant P53) have been shown to potentiate the activity of SREBP proteins (Freed-Pastor et al., 2012; Mullen et al., 2016). It has been difficult to advance small molecule inhibitors targeting the Wnt–β-catenin signaling pathway to clinical trials because of the important physiological functions of this pathway in normal cells. In this study, we found that HMGCR is a novel target gene of the β-catenin–TCF complex. Therefore, the use of statin to target tumors driven by the hyperactivation of β-catenin–TCF signaling might be a promising alternative strategy.

MATERIALS AND METHODS

Cell culture

Cells used in this study were obtained from the Cell Bank of the Type Culture Collection of the Chinese Academy of Sciences. A549, IOSE80, and Ovca429 cells were cultured in RPMI 1640 medium (Invitrogen) supplemented with 10% FBS. 293T, 4T1, Hepa1-6, Bease-2B, HPDE6C7, and Capan-1 cells were cultured in DMEM (Invitrogen) supplemented either with 10% FBS. NIH3T3 cells and MEFs were cultured with 10% new calf serum. All cells were supplemented with 10 U/ml penicillin G and incubated at 37°C in a humidified atmosphere containing 5% CO_2.

Mice

Pdx-Cre mice, *LSL-Kras*^{G12D} mice, and *Tg737*$^{loxp/loxp}$ mice were obtained from the Jackson Laboratory. All mice were in C57BL/6 background. The experimental animals were generated by crossing *Pdx-Cre* mice with mice expressing LSL-*Kras*^{G12D} and/or *Tg737*$^{loxp/loxp}$. All animal experiments were performed under the approval of the Institutional Animal Care and Use Committee.

Cilia staining

Cells were cultured on glass coverslips. After starvation for 2 d, the cells were fixed with prechilled methanol at −20°C for 5 min. For tissue staining, tissue samples were deparaffinized and fixed with 4% paraformaldehyde at 4°C for 30 min, followed by antigen retrieval in sodium citrate at 98°C for 30 min. The following procedure was performed according to standard protocol: in brief, after washing in PBS, the cells were blocked with PBS containing 3% BSA for 30 min at room temperature and then incubated with antiacetylated tubulin (1:1,000; Sigma), anti–γ-tubulin (1:1,000; Sigma), and anti-Kif3a (1:2,000; Abcam) antibodies in blocking buffer overnight at 4°C, followed by incubation with a 1:1,000 dilution of the corresponding secondary (Alexa Fluor 488/546 conjugated) antibody in blocking buffer at room temperature for 120 min. Hoechst staining (1:2,000 in PBS) was performed to label the nucleus. Fluorescence was monitored via inverted confocal laser microscopy (Carl Zeiss).

Transformation of NIH3T3 and HPDE6C7 cells

E1A–H-Ras was cloned into the retrovirus-producing vector pBabe, and NIH3T3 cells were incubated with the retrovirus expressing E1A–H-Ras according to the manufacturer's instructions. Similarly, K-RasV^{12} was cloned into the P23 vector, and the lentivirus was prepared according to the manufacturer's instructions. Cells able to form colonies on soft agar were considered to be transformed and were used in subsequent experiments.

Soft agar, focus formation, and colony formation assays

For the soft agar assay, 2,000 cells/well were plated in 24-well, flat-bottomed plates using a two-layer soft agar system in a volume of 400 µl/well. After 14 d of incubation, colonies were counted and measured. For focus formation, 10^5 cells were plated in 6-well plates. After reaching 90–100% confluence, the cells were incubated in a medium containing 5% serum for 2 wk. For the colony formation assay, 5×10^3 cells were plated in 6-well plates for 1 wk. The cells were then stained

were examined via immunohistochemical staining and assessed via linear regression (n = 21 for Hmgcr vs. Muc5 score; n = 18 for Hmgcr vs. β-catenin; n = 16 for Muc5 vs. β-catenin). **(F)** Correlations between the percentage of ciliated cells and the expression of Hmgcr, β-catenin, and Muc5 (n = 20). The expression of cilia, Hmgcr, β-catenin, and Muc5 in each individual was examined using immunostaining, and the correlations were assessed through linear regression. (E and F) Spearman correlation analysis was performed. The data are presented as the mean ± SEM. Representative data are of at least two independent experiments.

A

Gene	Normal Ct (18S-Gene)	Cancer Ct (18S-Gene)	*P* Value	Gene	Normal Ct (18S-Gene)	Cancer Ct (18S-Gene)	P Value
ACAT2	-16.23±0.3369	-15.28±0.2661	0.0299 *	HMGCS	-15.72±0.2311	-14.75±0.2225	0.03 *
ACLY	-15.34±0.2112	-14.35±0.1858	0.006 **	IDI1	-16.41±0.2308	-15.23±0.1903	0.0001 **
CYP51	-15.47±0.2476	-14.31±0.1868	0.003 **	MVD	-19.18±0.3941	-17.87±0.3957	0.0206 *
FDPS	-13.53±0.2846	-12.97±0.2287	0.127	NSDHL	-16.03±0.2492	-15.21±0.2440	0.0198 *
HMGCR	-17.61±0.3117	-16.59±0.2472	0.0124 *				

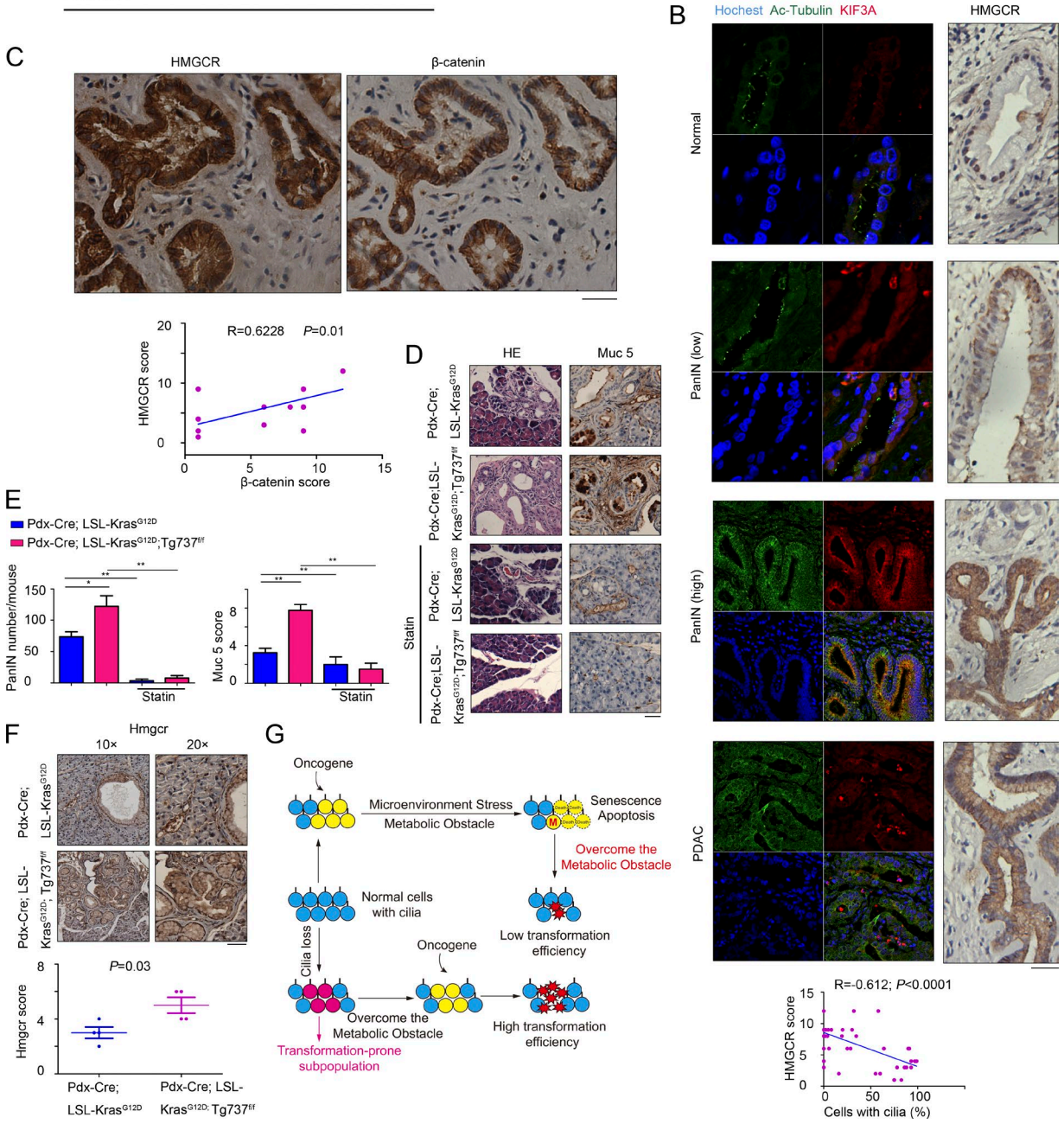

Figure 7. **Disruption of ciliogenesis is correlated with the activation of the MVA pathway in human PDAC samples. (A)** Up-regulation of enzymes in the MVA pathway in clinical PDAC samples. The expression of nine enzymes in the MVA pathway was examined in 64 clinical PDAC samples (n = 64) and noncancerous tissues (n = 64) using real-time PCR. 18S was used as an internal control. **(B)** Representative cilia staining and HMGCR expression data in

with crystal violet (0.5 g in 10% methanol) for 3 min and dissolved with 1% SDS. The OD value was measured at 600 nm.

RNA interference (RNAi) for Tg737 and Kif3a

The target sequences of the siRNAs for mouse Tg737and Kif3a and human Tg737 and KIF3A, as well as the randomly aligned sequence used as a negative control, are listed in Table S4. The FG12 lentiviral vector was used to produce double-stranded siRNAs. This vector system and its use have been described previously (Deng et al., 2007). The RNAi lentivirus particles used to knock down the expression of β-catenin were purchased from GeneChem (China). Cells were incubated with the lentivirus particles for 24 h and then sorted via flow cytometry using GFP as a marker.

Nuclease-deficient CRISPR-Cas9 (dCas9)

sgRNAs were designed to mediate a 20-nt base match with the TBE2 region of human HMGCR promoter (sgRNA for TBE2 dCas9 2: 5′-TATGTTCTCTTTGTTTACCT-3′; sgRNA for TBE2 dCas9 5: 5′-CAAAGAGAACATAAG CAGGG-3′) and cloned into a U6 promoter–driven expression plasmid (pGL3-U6-puro). The human codon–optimized Cas9 expression vector (44758; Addgene) was used as a template to generate the dCas9 (D10A, H840A) plasmid. For estimating the binding efficiency of dCas9/sgRNA, we used Cas9/sgRNA to generate mutations at target sites and performed a T7EN1 assay. Then, HPDE6C7 cells were cotransfected with 1.5 μg dCas9 plasmid and 2 μg of confirmed sgRNA plasmids. The binding efficiency was evaluated using a ChIP assay.

In vivo tumorigenicity assay

Male nude mice were housed under standard conditions. The animal protocols were performed in agreement with the Shanghai Institutes for Biological Science Guide for the Care and Use of Laboratory Animals and were approved by the Animal Care and Use Committee of the Shanghai Institutes for Biological Sciences. 4-wk-old male nude mice were subcutaneously injected with 10^6 cells per flank in both flanks. The resultant tumors were measured with calipers every 3 d, and tumor volume (millimeters cubed) was calculated using the standard formula length × width × height × 0.5236. At the end of the experiments, the tumors were harvested and weighed.

Microarray analysis

The total RNA was extracted from cells using TRIzol reagent. Microarray experiments and the subsequent expression analysis were performed according to the technical manual of the Affymetrix GeneChip (CapitalBio).

Western blot and real-time PCR analyses

The concentrations of protein samples extracted from the tissue specimens and cell lines in radioimmunoprecipitation assay lysis buffer were determined using the Bradford reagent (Sigma) according to the manufacturer's instructions. Western blot analysis was performed using a standard protocol. The following antibodies were used: rabbit anti-Tg737 (1:2,000; Protein Tech), anti-Kif3a (1:2,000; Abcam), anti-SREBP2 (1:3,000; Abcam), anti-HMGCR (HPA008338; Sigma), antitotal ERK (1:1,000; Cell Signaling Technology), anti-phosphorylated ERK (1:1,000; Cell Signaling Technology), anti–β-catenin (1:1,000; Cell Signaling Technology), anti-Ras (1:3,000; BD Bioscience), antitubulin (1:3,000; Santa Cruz), and anti-GAPDH (1:3,000; Santa Cruz). Total RNA was extracted from the cells using TRIzol according to the standard protocol. 2 μg RNA was processed directly into cDNA using a reverse transcription kit (Promega) according to the manufacturer's instructions. Amplification reactions were performed and relative gene expression levels were calculated as previously described (Deng et al., 2007). The primers used in these experiments are listed in Table S5.

Cell cultures and statin treatment

Statin was purchased from Sigma. Before treatment, statin was activated in 70% ethanol containing 0.1 N NaOH at 50°C for

normal pancreatic tissues, PanIN lesions, and PDAC samples. The correlations between the expression of HMGCR and the percentage of ciliated cells in PDAC tissues from each individual ($n = 34$) were examined via immunostaining and assessed via linear regression. **(C)** Representative immunohistochemical data for β-catenin and HMGCR expression in PDAC samples ($n = 11$). The correlation between the expression of HMGCR and β-catenin in PDAC tissues from each individual was examined via immunostaining and assessed via linear regression. (B and C) Spearman correlation analysis was performed. **(D)** Disruption of ciliogenesis promoted the formation of PanIN driven by oncogenic Ras, which was inhibited by statin. The pancreatic tissues of 8-mo-old *Pdx-Cre; Kras^{G12D}* mice and *Pdx-Cre; Tg737$^{loxp/loxp}$; Kras^{G12D}* mice that had been treated with lovastatin for 6 mo (20 mg/kg, twice for each week; intragastric administration) were harvested, after which hematoxylin and eosin (HE) staining was performed, and PanIN lesions and the expression of Muc5 were examined ($n = 4$ for each group). **(E)** Statistic analysis of data presented in D ($n = 4$ for each group). The data are presented as the mean ± SEM. **(F)** The expression of Hmgcr in the pancreatic tissues indicated in D was examined using immunohistochemistry ($n = 4$ for each group). (B–F) Bars, 40 μm. *, $P < 0.05$; **, $P < 0.01$. Representative data are of at least two independent experiments. **(G)** Model for the mechanism by which disrupted ciliogenesis sensitized cells to transformation. During the initial process through which normal cells are transformed, cells would be under severe microenvironmental stress (e.g., a shortage of oxygen and nutrients) and unable to overcome metabolic obstacles. Therefore, most of the cells would undergo senescence or apoptosis, and only a very small fraction of the cells would successfully achieve malignant transformation by gaining other mutations, enabling them to overcome the metabolic obstacles. Under these conditions, transformation efficiency is low. In contrast, the disruption of ciliogenesis would reprogram metabolic pathways, for example, activating the MVA pathway, causing these cells to become a transformation-prone subpopulation and sensitizing them to further transformation induced by additional genetic changes. Student's *t* was performed.

60 min and then neutralized with 70% ethanol containing 0.1 N HCl. Activated statin, either alone or in combination with FPP or GGPP (Sigma), was added to the medium the day after cells were plated, and the medium was changed every day.

Crystal violet assay

The crystal violet assay was performed to examine cell growth. Equal numbers of control cells and experimental cells were seeded in 12-well plates and cultured in medium supplemented with 10% FBS at a density of 1,000 cells/well. The medium was changed every other day. After 2 wk of culture under standard conditions, the medium was removed, and the cells were stained with a 0.5% crystal violet solution in 20% methanol. After staining for 10 min, the fixed cells were washed with PBS and photographed. The cells were subsequently dissolved with 1% SDS, and the OD was measured at 600 nm.

Tumorigenesis assay and statin treatment

4-wk-old male nude mice were obtained from the Slac Laboratory Animal Center. The animals were housed in sterile filter-capped microisolator cages and provided with sterilized food and water. To induce subcutaneous xenograft tumors, cells (2×10^6 cells/0.1 ml per site) suspended in 50% Matrigel in DMEM were subcutaneously injected into the flanks of the mice. After 3 d, the mice were administered vehicle or 50 mg/kg lovastatin every 2 d. 4 wk later, the tumors were harvested, and tumor weights were measured. All animal experiments were conducted under protocols approved by the Institutional Animal Care and Use Committee of the Shanghai Institutes for Biological Science.

Statin treatment was initiated in the PDAC mouse model when the mice were 2 mo old and ended when the mice were 8 mo old. Then, the pancreatic tissues were harvested and examined. Statin was administered intragastrically every 2 d (25 mg/kg), based on the animals' body weights.

Immunohistochemistry

Tissues (mouse pancreatic tissues, human pancreatic cancer tissues, and paired noncancerous tissues) were fixed in formalin, embedded in paraffin, and cut into 5-µm-thick consecutive sections. This study was approved by the ethics committee of the Institute for Nutritional Science, Chinese Academy of Science. After deparaffinization and antigen recovery (in sodium citrate solution, pH 6.0, for 20 min at 98°C), the sections were washed three times in 0.01 mol/L PBS (8 mmol/L Na_2HPO_4, 2 mmol/L NaH_2PO_4, and 150 mmol/L NaCl) for 5 min each, blocked for 1 h in 0.01 mol/L PBS containing 0.3% Triton X-100 and 5% BSA, and incubated with the HMGCR antibody (HPA008338; Sigma), CYP51 (Epitomics), MUC5 (Sigma), and β-catenin (Cell Signaling Technology) overnight at 4°C. After brief washes with 0.01 mol/L PBS, the sections were incubated with 0.01 mol/L PBS containing HRP-conjugated IgG (1:500) for 2 h, followed by development with 0.003% H_2O_2 and 0.03% 3,3′-diaminobenzidine in 0.05 mol/L Tris-HCl, pH 7.6. The immunohistochemistry for each sample was repeated three times.

A German semiquantitative scoring system was used to evaluate the expression of Muc5, β-catenin, and Hmgcr in the immunohistochemistry sections based on the staining intensity and area. In general, each specimen was assigned a score according to the intensity of staining (0 = no staining, 1 = weak staining, 2 = moderate staining, and 3 = strong staining) and the percentage of stained cells (0 = 0%, 1 = 1–24%, 2 = 25–49%, 3 = 50–74%, and 4 = 75–100%). The final immunoreactive score was determined by multiplying the intensity score with the score for the percentage of stained cells. As a result, nine grades were scored as 0, 1, 2, 3, 4, 6, 8, 9, and 12, and the scores were subsequently analyzed.

GST pull-down assay

Ras activation was assessed based on specific binding of Ras–guanosine triphosphate (GTP; activated form) to the RBD of Raf-1. The RBD (Raf-1 residue 1–149) was expressed as a GST fusion protein. The pGEX-RBD plasmid, encoding the RBD (amino acids 1–149) of Raf-1 fused with a GST tag, was transfected into *Escherichia coli*. The expression of the GST-RBD protein was induced with 1 mM isopropyl-β-D-thiogalactopyranoside for 2 h at 37°C. *E. coli* were then harvested and resuspended in a solution containing 20 mM Hepes, pH 7.5, 120 mM NaCl, 10% glycerol, 2 mM EDTA, and 10 µg/ml each of leupeptin, aprotinin, and pepstatin A. The cells were lysed via sonication and centrifuged at 14,000 rpm at 4°C for 15 min. The supernatants were incubated with glutathione-Sepharose beads for 1 h at 4°C, and the beads coupled with GST-RBD were washed six times with lysis buffer containing 0.5% NP-40. The bound GST-RBD was eluted by boiling in SDS sample buffer, and the concentration was determined by separating the proteins on SDS-PAGE gels with Coomassie brilliant blue staining.

For the measurement of Ras-GTP, cells were incubated with lysis buffer containing 25 mM Hepes, pH 7.5, 150 mM NaCl, 1% NP-40, 0.25% sodium deoxycholate, 10% glycerol, 25 mM NaF, 10 mM $MgCl_2$, 1 mM EDTA, 1 mM sodium vanadate, and 10 µg/ml each of leupeptin, aprotinin, and pepstatin A for 15 min at 4°C. The proteins in the lysate (500 µg) were incubated with an equal amount of GST-RBD that had been precoupled with glutathione-Sepharose at 4°C for 2 h. The bound proteins were eluted by boiling with SDS Laemmli buffer and then were subjected to electrophoresis via 12% SDS-PAGE and transferred to a nitrocellulose membrane. For immunoblotting, a monoclonal anti-Ras antibody was used as the primary antibody, and an HRP-conjugated anti–mouse IgG was used as the secondary antibody. After Western blotting, enhanced chemiluminescence (Pierce) was used for detection according to the manufacturer's protocol.

Luciferase assay

The GLISB-Luc, Topflash, and Fopflash reporters were purchased from Addgene. The promoters for human HMGCR

(−2,212 to −1), HMGCS (−3,067 to −1), CYP51 (−2,064 to −1), IDI1 (−2,306 to −1), and mouse Hmgcr (−2,448 to −1) were amplified from the genome DNA and inserted into the pGL3-basic plasmid. Cells were plated at a subconfluent density and cotransfected with 0.05 µg of the reporter plasmid, 0.5 µg of the expression vectors, and 0.05 µg of the *Renilla reniformis* luciferase pRL-TK plasmid as an internal control for transfection efficiency. Cell lysates were prepared 24 h after transfection, and reporter activity was measured using a Dual-Luciferase Reporter Assay System (Promega). For the LiCl treatment, 25 mM LiCl was added into the medium 8 h before the cells were harvested. Transfections were performed in triplicate and repeated three times to ensure reproducibility.

ChIP assay

Kits used to perform ChIP were provided by Cell Signaling Technology. Approximately 6×10^6 cells were used for each ChIP assay. The cells were cross-linked with 1% formaldehyde in PBS at room temperature for 10 min. Cross-linking was stopped by adding 1.0 M glycine to a final concentration of 125 mM, followed by incubation at room temperature for 5 min. The cells were then washed twice with ice-cold PBS and scraped into ice-cold PBS containing proteinase inhibitors (Roche Applied Science). The cells were subsequently collected and resuspended in lysis buffer (20 mM Hepes, pH 7.9, 420 mM NaCl, 0.2 mM EDTA, 0.5% NP-40, 25% glycerol, and 1.5 mM $MgCl_2$) containing proteinase inhibitors. The lysate was subjected to sonication to shear the chromatin into 200–1,000-bp fragments. One third of the lysate was incubated with 5 M NaCl at 65°C to reverse the cross-linking, followed by phenol/chloroform extraction, ethanol precipitation, and storage at −80°C as the input control for PCR analysis. The remaining two thirds of the lysate were subjected to immunoprecipitation with an anti–β-catenin antibody (Cell Signaling Technology), SREBP2 (Abcam), or IgG (Pierce). The immunoprecipitated complexes were collected using protein G–Sepharose beads. The precipitants were sequentially washed three times with lysis buffer. After the final wash, 300 µl of elution buffer (0.1 M $NaHCO_3$ and 1% SDS) was added, and the beads were rotated at room temperature for 15 min. 5 M NaCl was added to reverse the formaldehyde cross-linking. Finally, DNA was extracted with phenol/chloroform, ethanol precipitated, and resuspended in double-distilled water for PCR analysis. The sequences for the primers are listed in Table S5.

Statistical analysis

The experiments were performed in triplicate. Data are presented as means ± SEM. Statistical comparisons between groups were performed with Student's *t* test. ANOVA was used for multiple comparisons of data. Statistical analysis was performed with Prism v5.03 (GraphPad). Statistic differences were defined as *, $P < 0.05$ and **, $P < 0.01$.

Study approval

The protocol for tissue collection was approved by the Ethics Committee of Zhongshan Hospital (Fudan University) and by patients' written informed consent. All animal experiments were approved by the Institute for the Nutritional Science Committee and were in accordance with the National Policy on Humane Care and Use of Laboratory Animals.

Online supplemental material

Fig. S1 shows that the restoration of Vhl expression rescues ciliogenesis in transformed cells and disruption of ciliogenesis sensitizes cells to transformation by Ras and LT. Fig. S2 shows that cilia loss promotes the growth of MEFs through activation of the MVA pathway. Fig. S3 shows that β-catenin activates the expression of enzymes in the MVA pathway. Fig. S4 depicts cilia loss and activation of the MVA pathway in *Pdx-Cre; KrasG12D* mice. Table S1 shows the alteration of gene expression induced by the disruption of cilia. Table S2 shows the correlation between the expression of HEF1 and MVA enzymes in pancreatic cancer. Table S3 shows the correlation between the expression of Aurora A and MVA enzymes in adrenocortical carcinoma and ovarian serous cystadenocarcinoma. Table S4 lists target sequence for siRNA. Table S5 lists the primers used for real-time PCR.

ACKNOWLEDGMENTS

This work was supported partly by National Natural Science Foundation of China grants 81230058, 81730083, 31520103907, 81572750, and 81372289, Youth Innovation Promotion Association of Chinese Academy of Sciences fund 1731517600313-14, and the Shanghai Institutes for Biological Science fund 2014KIP105.

The authors declare no competing financial interests.

Author contributions: Y.-Z. Deng, Z. Cai, and D. Xie designed the experiments and wrote the paper. S. Shi, H. Jiang, Y.-R. Shang, and N. Ma performed the xenograft tumor experiments. J.-J. Wang, L.-M. Liu, and Y.-F. Rong processed clinical specimens. D. Feng and Q.-L. Zhou performed the ChIP experiments. D.-X. Guan and T.-W. Chen performed the real-time PCR experiments. E.-B. Zhang and Z.-Y. Qian performed immunohistochemical and pathological analysis. Y.-N. Du and X.-X. Huang worked with the dCas9 system. E. Chin, D.-P. Liu, X.-L. Zhang, D.-S. Li, and X.-F. Wang provided helpful discussion.

Submitted: 2 March 2017

Revised: 11 September 2017

Accepted: 23 October 2017

REFERENCES

Acs, P., P.O. Bauer, B. Mayer, T. Bera, R. Macallister, E. Mezey, and I. Pastan. 2015. A novel form of ciliopathy underlies hyperphagia and obesity in Ankrd26 knockout mice. *Brain Struct. Funct.* 220:1511–1528. https://doi.org/10.1007/s00429-014-0741-9

Bardou, M., A. Barkun, and M. Martel. 2010. Effect of statin therapy on colorectal cancer. *Gut.* 59:1572–1585. https://doi.org/10.1136/gut.2009.190900

Bridges, J.P., A. Schehr, Y. Wang, L. Huo, V. Besnard, M. Ikegami, J.A. Whitsett, and Y. Xu. 2014. Epithelial SCAP/INSIG/SREBP signaling regulates multiple biological processes during perinatal lung maturation. *PLoS One.* 9:e91376. https://doi.org/10.1371/journal.pone.0091376

Clendening, J.W., A. Pandyra, P.C. Boutros, S. El Ghamrasni, F. Khosravi, G.A. Trentin, A. Martirosyan, A. Hakem, R. Hakem, I. Jurisica, and L.Z. Penn. 2010. Dysregulation of the mevalonate pathway promotes

transformation. *Proc. Natl. Acad. Sci. USA.* 107:15051–15056. https://doi.org/10.1073/pnas.0910258107

Cuthbert, J.A., and P.E. Lipsky. 1995. Suppression of the proliferation of Ras-transformed cells by fluoromevalonate, an inhibitor of mevalonate metabolism. *Cancer Res.* 55:1732–1740.

D'Amico, A.V. 2010. Statin use and the risk of prostate-specific antigen recurrence after radiation therapy with or without hormone therapy for prostate cancer. *J. Clin. Oncol.* 28:2651–2652. https://doi.org/10.1200/JCO.2010.28.5809

Deng, Y.Z., P.P. Chen, Y. Wang, D. Yin, H.P. Koeffler, B. Li, X.J. Tong, and D. Xie. 2007. Connective tissue growth factor is overexpressed in esophageal squamous cell carcinoma and promotes tumorigenicity through beta-catenin-T-cell factor/Lef signaling. *J. Biol. Chem.* 282:36571–36581. https://doi.org/10.1074/jbc.M704141200

Freed-Pastor, W.A., H. Mizuno, X. Zhao, A. Langerød, S.H. Moon, R. Rodriguez-Barrueco, A. Barsotti, A. Chicas, W. Li, A. Polotskaia, et al. 2012. Mutant p53 disrupts mammary tissue architecture via the mevalonate pathway. *Cell.* 148:244–258. https://doi.org/10.1016/j.cell.2011.12.017

Gordan, J.D., C.B. Thompson, and M.C. Simon. 2007. HIF and c-Myc: sibling rivals for control of cancer cell metabolism and proliferation. *Cancer Cell.* 12:108–113. https://doi.org/10.1016/j.ccr.2007.07.006

Gruenbacher, G., and M. Thurnher. 2015. Mevalonate metabolism in cancer. *Cancer Lett.* 356(2, 2 Pt A):192–196. https://doi.org/10.1016/j.canlet.2014.01.013

Gutt, R., N. Tonlaar, R. Kunnavakkam, T. Karrison, R.R. Weichselbaum, and S.L. Liauw. 2010. Statin use and risk of prostate cancer recurrence in men treated with radiation therapy. *J. Clin. Oncol.* 28:2653–2659. https://doi.org/10.1200/JCO.2009.27.3003

Han, Y.G., H.J. Kim, A.A. Dlugosz, D.W. Ellison, R.J. Gilbertson, and A. Alvarez-Buylla. 2009. Dual and opposing roles of primary cilia in medulloblastoma development. *Nat. Med.* 15:1062–1065. https://doi.org/10.1038/nm.2020

Hanahan, D., and R.A. Weinberg. 2011. Hallmarks of cancer: the next generation. *Cell.* 144:646–674. https://doi.org/10.1016/j.cell.2011.02.013

Hingorani, S.R., E.F. Petricoin, A. Maitra, V. Rajapakse, C. King, M.A. Jacobetz, S. Ross, T.P. Conrads, T.D. Veenstra, B.A. Hitt, et al. 2003. Preinvasive and invasive ductal pancreatic cancer and its early detection in the mouse. *Cancer Cell.* 4:437–450. https://doi.org/10.1016/S1535-6108(03)00309-X

Hsu, P.P., and D.M. Sabatini. 2008. Cancer cell metabolism: Warburg and beyond. *Cell.* 134:703–707. https://doi.org/10.1016/j.cell.2008.08.021

Israelsen, W.J., and M.G. Vander Heiden. 2010. ATP consumption promotes cancer metabolism. *Cell.* 143:669–671. https://doi.org/10.1016/j.cell.2010.11.010

Jawaid, S., M. Gertz, C. Corsino, J. Cheung, H. Seidle, and R.D. Couch. 2010. Human hydroxymethylglutaryl-coenzyme A reductase (HMGCR) and statin sensitivity. *Indian J. Biochem. Biophys.* 47:331–339.

Karlic, H., R. Thaler, C. Gerner, T. Grunt, K. Proestling, F. Haider, and F. Varga. 2015. Inhibition of the mevalonate pathway affects epigenetic regulation in cancer cells. *Cancer Genet.* 208:241–252. https://doi.org/10.1016/j.cancergen.2015.03.008

Lancaster, M.A., J. Schroth, and J.G. Gleeson. 2011. Subcellular spatial regulation of canonical Wnt signalling at the primary cilium. *Nat. Cell Biol.* 13:700–707. https://doi.org/10.1038/ncb2259

Lu, W., H. Pelicano, and P. Huang. 2010. Cancer metabolism: is glutamine sweeter than glucose? *Cancer Cell.* 18:199–200. https://doi.org/10.1016/j.ccr.2010.08.017

Lutz, M.S., and R.D. Burk. 2006. Primary cilium formation requires von hippel-lindau gene function in renal-derived cells. *Cancer Res.* 66:6903–6907. https://doi.org/10.1158/0008-5472.CAN-06-0501

Lyssiotis, C.A., and L.C. Cantley. 2012. SIRT6 puts cancer metabolism in the driver's seat. *Cell.* 151:1155–1156. https://doi.org/10.1016/j.cell.2012.11.020

Michaud, E.J., and B.K. Yoder. 2006. The primary cilium in cell signaling and cancer. *Cancer Res.* 66:6463–6467. https://doi.org/10.1158/0008-5472.CAN-06-0462

Mok, C.A., E. Héon, and M. Zhen. 2010. Ciliary dysfunction and obesity. *Clin. Genet.* 77:18–27. https://doi.org/10.1111/j.1399-0004.2009.01305.x

Mullen, P.J., R. Yu, J. Longo, M.C. Archer, and L.Z. Penn. 2016. The interplay between cell signalling and the mevalonate pathway in cancer. *Nat. Rev. Cancer.* 16:718–731. https://doi.org/10.1038/nrc.2016.76

Nam, D.H., H. Lee, J.C. Park, S.K. Shin, S.K. Lee, W.J. Hyung, Y.C. Lee, M.W. Kang, and S.H. Noh. 2014. Long-term statin therapy improves oncological outcome after radical gastrectomy for stage II and III gastric cancer. *Anticancer Res.* 34:355–361.

Pal, K., and S. Mukhopadhyay. 2015. Primary cilium and sonic hedgehog signaling during neural tube patterning: role of GPCRs and second messengers. *Dev. Neurobiol.* 75:337–348. https://doi.org/10.1002/dneu.22193

Pampliega, O., I. Orhon, B. Patel, S. Sridhar, A. Díaz-Carretero, I. Beau, P. Codogno, B.H. Satir, P. Satir, and A.M. Cuervo. 2013. Functional interaction between autophagy and ciliogenesis. *Nature.* 502:194–200. https://doi.org/10.1038/nature12639

Pandyra, A.A., P.J. Mullen, C.A. Goard, E. Ericson, P. Sharma, M. Kalkat, R. Yu, J.T. Pong, K.R. Brown, T. Hart, et al. 2015. Genome-wide RNAi analysis reveals that simultaneous inhibition of specific mevalonate pathway genes potentiates tumor cell death. *Oncotarget.* 6:26909–26921. https://doi.org/10.18632/oncotarget.4817

Perera, R.M., S. Stoykova, B.N. Nicolay, K.N. Ross, J. Fitamant, M. Boukhali, J. Lengrand, V. Deshpande, M.K. Selig, C.R. Ferrone, et al. 2015. Transcriptional control of autophagy-lysosome function drives pancreatic cancer metabolism. *Nature.* 524:361–365. https://doi.org/10.1038/nature14587

Popják, G., C.F. Clarke, C. Hadley, and A. Meenan. 1985. Role of mevalonate in regulation of cholesterol synthesis and 3-hydroxy-3-methylglutaryl coenzyme A reductase in cultured cells and their cytoplasts. *J. Lipid Res.* 26:831–841.

Praetorius, H.A., J. Praetorius, S. Nielsen, J. Frokiaer, and K.R. Spring. 2004. Beta1-integrins in the primary cilium of MDCK cells potentiate fibronectin-induced Ca2+ signaling. *Am. J. Physiol. Renal Physiol.* 287:F969–F978. https://doi.org/10.1152/ajprenal.00096.2004

Pugacheva, E.N., S.A. Jablonski, T.R. Hartman, E.P. Henske, and E.A. Golemis. 2007. HEF1-dependent Aurora A activation induces disassembly of the primary cilium. *Cell.* 129:1351–1363. https://doi.org/10.1016/j.cell.2007.04.035

Rohatgi, R., L. Milenkovic, and M.P. Scott. 2007. Patched1 regulates hedgehog signaling at the primary cilium. *Science.* 317:372–376. https://doi.org/10.1126/science.1139740

Schneider, L., M. Cammer, J. Lehman, S.K. Nielsen, C.F. Guerra, I.R. Veland, C. Stock, E.K. Hoffmann, B.K. Yoder, A. Schwab, et al. 2010. Directional cell migration and chemotaxis in wound healing response to PDGF-AA are coordinated by the primary cilium in fibroblasts. *Cell. Physiol. Biochem.* 25:279–292. https://doi.org/10.1159/000276562

Seeger-Nukpezah, T., J.L. Little, V. Serzhanova, and E.A. Golemis. 2013. Cilia and cilia-associated proteins in cancer. *Drug Discov. Today Dis. Mech.* 10:e135–e142. https://doi.org/10.1016/j.ddmec.2013.03.004

Seeley, E.S., C. Carrière, T. Goetze, D.S. Longnecker, and M. Korc. 2009. Pancreatic cancer and precursor pancreatic intraepithelial neoplasia lesions are devoid of primary cilia. *Cancer Res.* 69:422–430. https://doi.org/10.1158/0008-5472.CAN-08-1290

Tang, Z., M.G. Lin, T.R. Stowe, S. Chen, M. Zhu, T. Stearns, B. Franco, and Q. Zhong. 2013. Autophagy promotes primary ciliogenesis by removing OFD1 from centriolar satellites. *Nature.* 502:254–257. https://doi.org/10.1038/nature12606

Thoma, C.R., I.J. Frew, C.R. Hoerner, M. Montani, H. Moch, and W. Krek. 2007. pVHL and GSK3beta are components of a primary cilium-maintenance signalling network. *Nat. Cell Biol.* 9:588–595. https://doi.org/10.1038/ncb1579

Warita, K., T. Warita, C.H. Beckwitt, M.E. Schurdak, A. Vazquez, A. Wells, and Z.N. Oltvai. 2014. Statin-induced mevalonate pathway inhibition attenuates the growth of mesenchymal-like cancer cells that lack functional E-cadherin mediated cell cohesion. *Sci. Rep.* 4:7593. https://doi.org/10.1038/srep07593

Wejde, J., H. Blegen, and O. Larsson. 1992. Requirement for mevalonate in the control of proliferation of human breast cancer cells. *Anticancer Res.* 12:317–324.

Wong, W.W., J.W. Clendening, A. Martirosyan, P.C. Boutros, C. Bros, F. Khosravi, I. Jurisica, A.K. Stewart, P.L. Bergsagel, and L.Z. Penn. 2007. Determinants of sensitivity to lovastatin-induced apoptosis in multiple myeloma. *Mol. Cancer Ther.* 6:1886–1897. https://doi.org/10.1158/1535-7163.MCT-06-0745

Wu, J., W.W. Wong, F. Khosravi, M.D. Minden, and L.Z. Penn. 2004. Blocking the Raf/MEK/ERK pathway sensitizes acute myelogenous leukemia cells to lovastatin-induced apoptosis. *Cancer Res.* 64:6461–6468. https://doi.org/10.1158/0008-5472.CAN-04-0866

Xu, N., N. Shen, X. Wang, S. Jiang, B. Xue, and C. Li. 2015. Protein prenylation and human diseases: a balance of protein farnesylation and geranylgeranylation. *Sci. China Life Sci.* 58:328–335. https://doi.org/10.1007/s11427-015-4836-1